THE FASEB JOURNAL • RESEARCH • www.fasebj.org

Serine-47 phosphorylation of cytochrome *c* in the mammalian brain regulates cytochrome *c* oxidase and caspase-3 activity

Hasini A. Kalpage,[*] Asmita Vaishnav,[†] Jenney Liu,[*] Ashwathy Varughese,[*,†] Junmei Wan,[*,†] Alice A. Turner,[*,†] Qinqin Ji,[‡] Matthew P. Zurek,[*] Alexandr A. Kapralov,[§] Valerian E. Kagan,[§,¶] Joseph S. Brunzelle,[‖] Maurice-Andre Recanati,[*,#] Lawrence I. Grossman,[*] Thomas H. Sanderson,[,††,‡‡] Icksoo Lee,[§§] Arthur R. Salomon,[‡] Brian F. P. Edwards,[†] and Maik Hüttemann[*,†,‡‡,1]**

[*]Center for Molecular Medicine and Genetics, [†]Department of Biochemistry, Microbiology, and Immunology, and [#]Department of Obstetrics and Gynecology, Wayne State University, Detroit, Michigan, USA; [‡]Department of Chemistry, Brown University, Providence, Rhode Island, USA; [§]Department of Environmental and Occupational Health, Center for Free Radical and Antioxidant Health, University of Pittsburgh, Pittsburgh, Pennsylvania, USA; [¶]Laboratory of Navigational Redox Lipidomics, I. M. Sechenov Moscow Medical State University, Moscow, Russia; [‖]Center for Synchrotron Research, Northwestern University, Argonne, Illinois, USA; [**]Department of Emergency Medicine and [††]Department of Molecular and Integrative Physiology, University of Michigan Medical School, Ann Arbor, Michigan, USA; [‡‡]Cardiovascular Research Institute, Wayne State University School of Medicine, Detroit, Michigan, USA; and [§§]College of Medicine, Dankook University, Cheonan-si, South Korea

ABSTRACT: Cytochrome *c* (Cyt*c*) is a multifunctional protein that operates as an electron carrier in the mitochondrial electron transport chain and plays a key role in apoptosis. We have previously shown that tissue-specific phosphorylations of Cyt*c* in the heart, liver, and kidney play an important role in the regulation of cellular respiration and cell death. Here, we report that Cyt*c* purified from mammalian brain is phosphorylated on S47 and that this phosphorylation is lost during ischemia. We have characterized the functional effects *in vitro* using phosphorylated Cyt*c* purified from pig brain tissue and a recombinant phosphomimetic mutant (S47E). We crystallized S47E phosphomimetic Cyt*c* at 1.55 Å and suggest that it spatially matches S47-phosphorylated Cyt*c*, making it a good model system. Both S47-phosphorylated and phosphomimetic Cyt*c* showed a lower oxygen consumption rate in reaction with isolated Cyt*c* oxidase, which we propose maintains intermediate mitochondrial membrane potentials under physiologic conditions, thus minimizing production of reactive oxygen species. S47-phosphorylated and phosphomimetic Cyt*c* showed lower caspase-3 activity. Furthermore, phosphomimetic Cyt*c* had decreased cardiolipin peroxidase activity and is more stable in the presence of H_2O_2. Our data suggest that S47 phosphorylation of Cyt*c* is tissue protective and promotes cell survival in the brain.—Kalpage, H. A., Vaishnav, A., Liu, J., Varughese, A., Wan, J., Turner, A. A., Ji, Q., Zurek, M. P., Kapralov, A. A., Kagan, V. E., Brunzelle, J. S., Recanati, M.-A., Grossman, L. I., Sanderson, T. H., Lee, I., Salomon, A. R., Edwards, B. F. P, Hüttemann, M. Serine-47 phosphorylation of cytochrome *c* in the mammalian brain regulates cytochrome *c* oxidase and caspase-3 activity. FASEB J. 33, 13503–13514 (2019). www.fasebj.org

KEY WORDS: apoptosis · electron transport chain · ischemia · respiration · signaling

Cytochrome *c* (Cyt*c*) is a mitochondrial hemeprotein that plays a central role in cellular respiration and apoptosis. Cyt*c* takes part in respiration by transferring electrons from bc_1 complex (complex III) to cytochrome *c* oxidase (complex IV, COX) where oxygen is reduced to water in the electron transport chain (ETC). This is the proposed rate-limiting step of the ETC in intact cells (1, 2), with the free energy released during this reaction being twice as high compared with complexes I and III, making it effectively an irreversible reaction (3). The ETC complexes I, III, and IV pump protons across the mitochondrial inner membrane, generating an electrochemical gradient that is utilized by ATP synthase (complex V) to convert ADP and phosphate to ATP. Cyt*c* is not only an indispensable protein for cellular energy production but also a major signaling molecule for apoptosis. In the presence of an apoptotic signal, Cyt*c* is released from the mitochondria

ABBREVIATIONS: $\Delta\Psi_m$, mitochondrial membrane potential; Apaf-1, apoptotic protease activating factor 1; COX, cytochrome *c* oxidase; Cyt*c*, cytochrome *c*; DCIP, 2,6-dichloroindophenol; E°′, midpoint redox potential; ETC, electron transport chain; PDB, Protein Data Bank; RMSD, root mean square deviation; ROS, reactive oxygen species; WT, wild type

[1] Correspondence: Center for Molecular Medicine and Genetics, Wayne State University School of Medicine, 540 East Canfield St., Detroit, MI 48201, USA. E-mail: mhuttema@med.wayne.edu

doi: 10.1096/fj.201901120R
This article includes supplemental data. Please visit *http://www.fasebj.org* to obtain this information.

into the cytosol and interacts with the protein apoptotic protease activating factor 1 (Apaf-1) (4). This results in the formation of the apoptosome, which activates the caspase cascade, leading to cell death.

Furthermore, during the early process of apoptosis, Cyt*c* functions as a peroxidase of cardiolipin, a mitochondria-specific lipid that interacts with Cyt*c* (5, 6). About 15–20% of Cyt*c* is tethered to cardiolipin (7, 8). Cyt*c* acts as a catalyst of cardiolipin peroxidation in the presence of reactive oxygen species (ROS) such as H_2O_2. In apoptotic cells, 60% of cardiolipin is redistributed to the outer mitochondrial membrane, facilitating Cyt*c* release from the mitochondria into the cytosol (9). Cyt*c* is also involved in both ROS production and scavenging, utilizing its ability to accept and donate electrons (10, 11). These multifunctional properties of Cyt*c* identify it as a cellular life and death decision molecule. Consequently, the protein is tightly regulated by allosteric mechanisms (ATP/ADP ratio), tissue-specific isoform expression, and reversible phosphorylations, as reviewed in Kalpage *et al*. (12).

Reversible phosphorylations of Cyt*c* take place in a highly tissue-specific manner on distinct sites in mammalian liver, heart, and kidney under basal conditions (13–15). We have previously reported that phosphorylation of brain Cyt*c* at Y97 is strongly induced by neuroprotective insulin treatment, but this Tyr phosphorylation is absent under basal conditions (16). In this study, we explored the basal phosphorylation state of brain Cyt*c* and identified a novel phosphorylation site on S47. Interestingly, this phosphorylation is lost under ischemia, which is an oxygen-depleted condition present in pathologies such as ischemic stroke. This modification of Cyt*c* was also identified in a number of high-throughput studies of the human skeletal muscle phosphoproteome (17, 18), but was not functionally characterized.

Most mammals including rodents have a somatic and a testes tissue-specific isoform of Cyt*c*. However, this testes-specific isoform was lost in primates and is only present as a nontranscribed pseudogene in humans (19). The sequence of human Cyt*c* is a mixture of both somatic and testes-specific isoforms of mammals that express the 2 isoforms (19, 20). Cyt*c*, together with its partner COX, is tightly regulated to meet the tissue-specific needs and energy demand of an organism. COX isoforms are known for subunits IV, VIa, VIb, VIIa, and VIII, which are reviewed (21, 22).

Here, we report that Cyt*c* purified from mammalian brain tissue is phosphorylated on S47 under basal conditions. This modification lowers respiration, apoptosis, and cardiolipin-induced peroxidase activity. However, under ischemic conditions, Cyt*c* becomes dephosphorylated, thus reversing all the neuroprotective functions of S47 phosphorylation. Our model proposes that cell signaling mechanisms that target Cyt*c* for phosphorylation control respiration to maintain intermediate mitochondrial membrane potentials ($\Delta\Psi_m$) (23, 24). Such regulation is crucial for higher organisms because $\Delta\Psi_m$ is directly related to ROS production. At $\Delta\Psi_m > 140$ mV, ROS production at ETC complexes I and III increases exponentially, whereas mitochondria of resting cells with a low $\Delta\Psi_m$ do not produce significant amounts of ROS (25–28). We propose that changes in the phosphorylation state of Cyt*c* in the context of brain ischemia-reperfusion provides a mechanism for brain reperfusion injury through maximal ETC flux, $\Delta\Psi_m$ hyperpolarization, and excessive ROS production, exacerbating tissue damage.

MATERIALS AND METHODS

Cyt*c* and COX purification

For Cyt*c* purification, pig brains were obtained from a slaughterhouse (Dunbar, Milan, MI, USA) and snap frozen. Half of the weighed brain tissue was left under ischemic conditions in a tightly sealed bag at 37°C for 1 h. All procedures involving animal tissues were approved by the Wayne State University Institutional Animal Care and Use Committee. The tissue incubated under ischemic conditions and nonischemic tissue were processed separately. Cyt*c* was purified using our established protocol (13–15) with minor modifications: Cyt*c* eluted from the CM52 cellulose column (GE Healthcare) was concentrated under vacuum to 1 ml and further purified by size exclusion using a Sephacryl S-100 (GE Healthcare) gel filtration column. Gel-filtered Cyt*c* was concentrated and buffer exchanged to water using Amicon Ultra-15 10 kDa centrifugal filter units (MilliporeSigma, Burlington, MA, USA).

Regulatory competent COX was purified from pig brain and heart as previously described for cow liver and heart COX under conditions that preserve phosphorylation (29) with minor modifications: additional washing steps with ST buffer (250 mM sucrose, 20 mM Tris, pH 7.4) were performed for the isolation of brain mitochondria because of the large amount of fat present in brain tissue compared with heart. To break the mitochondrial membranes, 20% Triton X-114 (1.5 ml/g protein) was added to brain mitochondria. Extracted COX was loaded onto a DEAE-Sepharose (GE Healthcare) anion-exchange column equilibrated with 125 mM KPi, 0.5% Triton X-100. COX was eluted using a salt gradient (100–700 mM KPi, 0.1% Triton X-100, pH 7.4). COX was further purified by ammonium sulfate precipitation as described in Lee *et al*. (29).

S47 phosphorylation mapping by mass spectrometry

The purified pig brain Cyt*c* was trypsin digested and enriched for phosphopeptides using the PhosTio Kit (GL Science, Tokyo, Japan). The peptides were eluted into a Linear-Trap Quadrupole Fourier Transform (LTQ-FT) Mass Spectrometer (Thermo Fisher Scientific, Waltham, MA, USA) through C18 reverse-phase gradient column chromatography followed by electrospray ionization as described in Sanderson *et al*. (16). The tandem mass spectrometry spectra were collected in the positive ion mode and assigned to peptide sequences. Phosphopeptides of interest were manually verified.

Site-directed mutagenesis

The codon corresponding to S47 of the somatic rodent Cyt*c* cDNA cloned into pLW01 expression vector (30) was mutagenized to a glutamate residue (S47E) as a phosphomimetic replacement and with an alanine residue as an additional control (S47A), which cannot be phosphorylated. These mutants were

generated using the QuickChange Lightning Site-Directed Mutagenesis Kit (Agilent Technologies, Santa Clara, CA, USA) according to the manufacturer's protocol. Briefly, the pLW01 Cyt*c* plasmid was amplified using the following mutagenesis primers. S47A forward: 5′-CCAGGCTGCTGGATTCGCTTACACAGATGCC-3′, S47A reverse: 5′ GGCATCTGTGTAAGCGAATCCAGCAGCCTGG-3′, S47E forward: 5′-CCAGGCTGCTGGATTCGAGTACACAGATGCC-3′, S47E reverse: 5′-GGCATCTGTGTACTCGAATCCAGCAGCCTGG-3′. The parental DNA was digested using *Dpn*I restriction enzyme, and the DNA was transformed into XL10-Gold ultracompetent cells. pLW01 plasmids were purified from individual colonies using the Wizard Plus SV Miniprep Purification System (Promega, Madison, WI, USA) and DNA sequencing was performed to confirm the presence of the desired mutation.

Bacterial overexpression and recombinant protein purification

Following sequence confirmation, the pLW01 plasmid was transformed into C41 (DE3) competent bacterial cells (Lucigen, Middleton, WI, USA). Bacterial colonies were cultured in Terrific Broth (Research Products International, Mount Prospect, IL, USA) medium with 0.1 mg/ml carbenicillin at 37°C and induced with 100 μM isopropyl-β-D-thiogalactoside when an optical density $(OD)_{600}$ of 1 was reached. The bacterial cells were harvested and lysed, and Cyt*c* was purified, as previously described in Mahapatra *et al*. (15), with slightly modified ion exchange chromatography conditions for the DE52 anion-exchange (pH 7.4, 4.0 mS/cm conductivity) column and CM52 cation exchange column (pH 6.5, 6.0 mS/cm conductivity). The protein was eluted with a high-salt elution buffer (40 mM KPi, 0.5 M NaCl). Cyt*c* was further purified by size exclusion chromatography and buffer exchanged to water as previously described for Cyt*c* purification from brain tissue.

Analysis of Cyt*c* spectra

Cyt*c* concentration was determined by the spectrophotometric method as previously described in Mahapatra *et al*. (15). Cyt*c* was oxidized and reduced with $K_3Fe(CN)_6$ and $Na_2S_2O_4$, respectively, and desalted using Sephadex G-25 NAP5 columns (GE Healthcare). The Cyt*c* concentration was calculated using the following equation: $(A_{550red} - A_{550oxi})/19.6\ mM/cm \times 1\ cm$ (31). Reduced Cyt*c* was used to obtain the spectrum from 220 to 700 nm. Oxidized Cyt*c* (100 μM) was used to obtain the spectrum from 600 to 750 nm to analyze the peak at 695 nm.

COX activity measurements

Purified pig brain COX was diluted to 3 μM, and cardiolipin (MilliporeSigma) was added to a 40:1 cardiolipin: COX molar ratio. The enzyme was dialyzed (MW cutoff: 12,000–14,000 Da) in COX measuring buffer [10 mM K-4-(2-hydroxyethyl)-1-piperazineethanesulfonic acid, pH 7.4, 40 mM KCl, 1% Tween 20, supplemented with 0.2 mM ATP] at 4°C overnight to remove bound cholate (15). Oxygen consumption was measured *via* a Clark-type oxygen electrode (Oxygraph System; Hansatech, Pentney, United Kingdom) at a final concentration of 54.5 nM brain COX and 163 nM heart COX in 220 μl measuring buffer. Ascorbate (20 mM) was added as an electron donor for Cyt*c*. Purified Cyt*c* (5 μM) was injected into the air-tight oxygen electrode. Oxygen consumption was recorded and analyzed using the Oxygraph software (Hansatech). COX activity was expressed as oxygen consumed per minute.

Caspase-3 activity assay

Cyt$c^{-/-}$ embryonic fibroblasts (CRL 2613; American Type Culture Collection, Manassas, VA, USA) were cultured in 8 T75 cell culture flasks. The cells were harvested, and a cytosolic extract was prepared as previously described in Mahapatra *et al*. (15). Enzchek Caspase-3 Assay Kit 2 (Thermo Fisher Scientific) containing the rhodamine 110-linked DEVD tetrapeptide that fluoresces upon cleavage by caspase-3 was used for caspase-3 activity measurements. Fluorescence was measured using a Fluoroskan Ascent FL plate reader (Thermo Fisher Scientific) using 485-nm excitation (14-nm bandwidth) and 527-nm emission (10-nm bandwidth) filters. The final readings were corrected for background fluorescence in the absence of Cyt*c*.

Redox potential measurement

The midpoint redox potential ($E°'$) was analyzed spectrophotometrically as previously described in Mahapatra *et al*. (15) using 2,6-dichloroindophenol (DCIP, $E°' = 237$ mV) as a reference compound. Data obtained were plotted as $\log(DCIP_{ox}/DCIP_{red})$ *vs.* $\log(Cyt_{ox}/Cyt_{red})$, yielding a linear graph with a slope of nDCIP/nCyt*c* and a *y* axis intercept of nCyt*c*/59.2(E Cyt*c* – *E* DCIP). These values were used to calculate the $E°'$ of Cyt*c* from the Nernst equation.

Heme degradation assay

Oxidized Cyt*c* variants were passed through NAP5 columns to remove the oxidant $K_3Fe(CN)_6$ and diluted to a final concentration of 5 μM in 50 mM phosphate buffer (pH 6.1). An excess of 3 mM H_2O_2 was added and the reduction of 408 nm heme Soret band of Cyt*c* was measured after 60 s as previously described in Liu *et al*. (32).

Cardiolipin peroxidase activity

Tetralinoleylcardiolipin and Cyt*c* (1 μM) of varying ratios (10:1, 20:1) were incubated for 10 min. Peroxidase activity was measured upon addition of Amplex red (50 μM) and H_2O_2 (50 μM) (15). Amplex red, when oxidized, is converted to resorufin. Resorufin fluorescence was measured at 535/585 nm (excitation/emission) using a "Fusion R" universal microplate analyzer.

Gel electrophoresis and Western blotting

Purified Cyt*c* was loaded on a 10% acrylamide (37.5:1) Tris-tricine gel, Coomassie stained for 1 h, and destained overnight. For Western blotting, the gel was transferred onto a PVDF membrane using a Bio-Rad *trans*-blot semidry transfer apparatus (125 mA, 25 V, 1 h). Membranes were blocked with 5% blocking reagent (bovine serum albumin for anti-phospho antibodies and dry milk for the Cyt*c* antibody) for 1 h and incubated with primary antibodies: Cyt*c* mouse monoclonal (BD Pharmingen, San Jose, CA, USA), 1:1000, and Ser phosphoantibody cocktail (4 monoclonal antibodies 1C8, 4A3, 4A9, and 16B4; EMD Biosciences, San Diego, CA, USA), 1:1000. After overnight primary antibody incubation, blots were washed with 1×Tris-buffered saline, 0.1% Tween 20 buffer and incubated with horseradish peroxidase–conjugated secondary mouse IgG (Cyt*c*) and mouse IgM (phosphoserine) antibodies in a 1:5000 dilution for 2 h. The blots were washed with 1× Tris-buffered saline, 0.1% Tween 20 following secondary antibody incubation and visualized with HyGlo chemiluminescent reagent (Denville Scientific, Holliston, MA, USA), using an automatic X-ray film processor, model JP-33.

Phostag gel electrophoresis

A Phostag (100 μM) AAL-107 ligand (Wako Chemicals, Richmond, VA, USA) containing 10% Tris-Tricine gel was cast according to the manufacturer's protocol. Tissue-purified Cyt*c* from both ischemic and nonischemic conditions was loaded with cow heart Cyt*c* (MilliporeSigma) as an additional control. The Phostag gel was run and immunoblotted with anti-rabbit Cyt*c* antibody (ab18738; Abcam, Cambridge, MA, USA). The Phostag gel was incubated in transfer buffer with 5 μM EDTA for 20 min before transfer to remove Mn^{2+}. The band intensity of phosphorylated and unphosphorylated Cyt*c* was quantified using the density-in-box tool of Quantity One 1-Dimension Analysis Software (Bio-Rad, Hercules, CA, USA), after correction for background.

High-resolution gel for separation of COX subunits

The COX subunits were separated by the Kadenbach SDS-PAGE-urea method (33). The separation gel solution had a final concentration of 16% acrylamide and 7.2 M urea. Purified heart and brain COX (30 μg/lane) were loaded, and the gel was run at 180 V overnight.

Statistical analysis

Experimental data consisting of 3 or more replicates were analyzed for statistical significance for the different experiments by a 2-sided Wilcoxon rank-sum test using MSTAT v.6.1. Data are reported as means ± SD and were considered statistically significant when $P < 0.05$.

Cyt*c* crystallization

S47E Cyt*c* was purified and crystallized using the same procedures employed successfully for 3 previous Cyt*c* structures (15). Briefly, it was gel-filtered on an S-100 column, concentrated to 15 mg/ml or higher in water, and oxidized with 5 mM $K_3Fe(CN)_6$ [Protein Data Bank (PDB): FC6] prior to crystallization. Crystals were grown by vapor diffusion after mixing 1 μl of protein solution with 1 μl of precipitant solution and equilibrating the drop against 0.5 ml of the precipitant at room temperature. The respective precipitant solutions are listed in Supplemental Table S1. The single crystal was soaked for 10 min in a cryo-protectant solution (Supplemental Table S1) before flash freezing in liquid nitrogen. Diffraction data were collected at the Life Sciences Collaborative Access Team facility (Advanced Photon Source sector 21; Argonne National Laboratory, Lemont, IL, USA). The data were integrated using XDS (34) in AutoProc (35). The structure was solved, rebuilt, refined, and analyzed using the Phenix (36) suite of programs (AutoMR, AutoBuild, Refine, Composite.Omit). The beginning model for AutoMR was chain-A of wild-type (WT) Cyt*c* (5C0Za). The 4 FC6 molecules were located in anomalous diffraction difference maps, and their occupancies were refined in Phenix. The final structure was optimized with PDB-REDO (37), which also refined the heme links to Cys14, Cys17, His18, and Met80 against standard bond values. This final step improved R_{work} by 2.2%, R_{free} by 1.7%, and the real space correlation coefficient for the electron density of 115/416 residues (none were worse).

Molecular dynamics

Molecular dynamics were performed with Yasara v.17-12-24 (38) using its conservative "slow" protocol, recommended defaults for all parameters, and the most recent force field, Amber 2014 (39). The starting structures for the molecular dynamics calculations on the S47 mutants were prepared from chain 5C0Za. Root mean square fluctuation and root mean square deviation (RMSD) plots were generated with Excel using data imported from Yasara. The "omit" electron density plots were assembled with PyMOL [The PyMOL Molecular Graphics System, v.2.2.3 (2018) Schrödinger, New York, NY, USA] using the simple "composite.omit" electron density calculated by Phenix. The final assembly of all figures was done in Photoshop (Adobe, San Jose, CA, USA).

RESULTS

Brain Cyt*c* is S47 phosphorylated and becomes dephosphorylated during ischemia

Previously, our lab identified distinct phosphorylation sites of Cyt*c* purified from the heart, liver, and kidney under basal conditions. However, the basal phosphorylation state of Cyt*c* in the brain was not known. Cyt*c* purified from pig brain tissue was found by Western analysis to be Ser phosphorylated (**Fig. 1*A***). The purified protein was properly folded and functional based on the presence of its characteristic α, β, and γ peaks (40) in the reduced absorption spectrum of Cyt*c* (Fig. 1*B*). Through mass spectrometry, we showed that the protein was phosphorylated at S47 (Fig. 1*C*), the only Ser residue present in porcine and rodent somatic Cyt*c*. This Ser phosphorylation was completely lost when Cyt*c* was isolated from brain tissue that was left ischemic for 1 h (**Fig. 2*A***).

Cyt*c* S47 phosphorylation inhibits respiration

To analyze the effect of this post-translational modification in reaction with COX, the corresponding COX enzyme was purified from porcine brain and from heart tissue as a control. These proteins were resolved in a high-resolution urea-polyacrylamide gel (33) to separate the 13 tightly bound subunits of COX (Fig. 2*B*).

The COX brain and heart enzymes differ by 3 tissue-specific isoforms of subunits VIa, VIIa, and VIII, which run at slightly different positions, with the heart COX containing the heart isoforms and the brain COX containing the liver-type isoforms (41). Using Cyt*c* purified from nonischemic (phosphorylated) and ischemic (dephosphorylated) brain tissue, oxygen consumption with the matching COX isozyme from pig brain was measured with a Clark-type oxygen electrode. The phosphorylated (nonischemic) form resulted in partial inhibition of respiration by 48% compared with dephosphorylated (ischemic) Cyt*c* (**Table 1**). This suggests that S47-phosphorylated (phospho-S47) Cyt*c* may regulate ETC electron flux to maintain healthy intermediate $\Delta\Psi_m$ levels under physiologic conditions (see Discussion).

Cyt*c* S47 phosphorylation inhibits apoptosis

The effect of Cyt*c* S47 phosphorylation on its second important function, apoptosis, was determined as a measure of caspase-3 activity. Caspase-3 is an executioner caspase

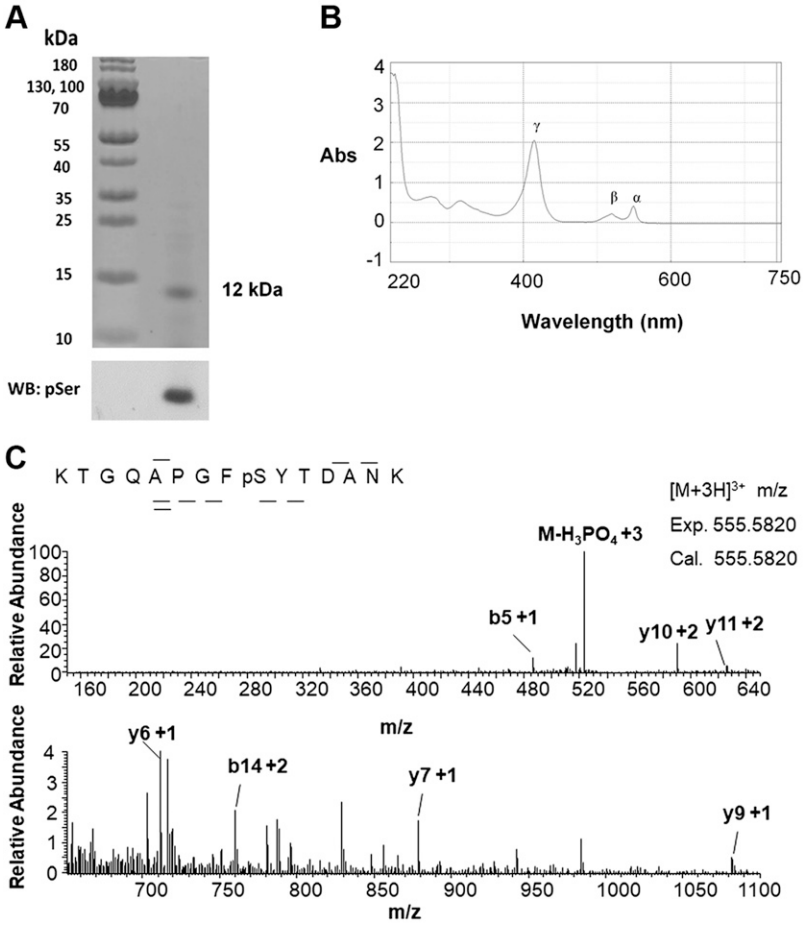

Figure 1. Cyt*c* purified from porcine brain tissue is phosphorylated at S47 under basal conditions. *A*) Purified porcine brain Cyt*c* is Ser phosphorylated. Top, Coomassie gel; bottom, anti-phosphoserine (pSer) Western blot (WB). *B*) The reduced absorption spectrum of porcine brain Cyt*c* (13 μM) showing its characteristic α (550–558), β (521–527), and γ (415–423) peaks. *C*) nano–liquid chromatography electrospray ionization tandem mass spectrometric spectrum of KTGQAPGFpSYTDANK indicates that porcine brain Cyt*c* is phosphorylated on S47. The phosphorylation site was unambiguously revealed by fragment ions y6 and y7. Abs, absorbance.

that acts as a terminal enzyme in the caspase cascade. Caspase-3 activity was measured using cytosolic extracts from Cyt*c* knockout mouse embryonic fibroblasts in combination with the artificial substrate DEVD-Rhodamine110, which fluoresces upon cleavage by active caspase-3. The apoptotic activity was significantly lower, by 62%, in the presence of phospho-S47 nonischemic Cyt*c*, as compared with dephosphorylated (ischemic) Cyt*c* (Table 1). In order to determine the proportion of Cyt*c* that is phosphorylated in the brain, the phosphorylated protein was separated from

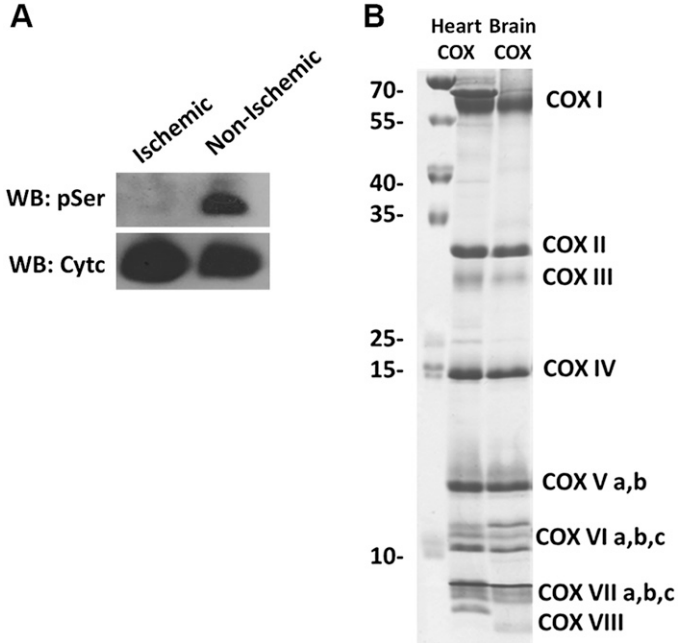

Figure 2. Cyt*c* purified from ischemic porcine brain tissue is dephosphorylated. *A*) Purified porcine brain Cyt*c* from ischemic tissue (lane 1) and normal, nonischemic tissue (lane 2). Top, immunoblot with phosphoserine (pSer) antibodies; bottom, immunoblot with a Cyt*c* antibody. *B*) COX purified from porcine heart (lane 1) and brain (lane 2) resolved on a high-resolution SDS-PAGE-urea gel showing all 13 tightly bound subunits of COX. WB, Western blot.

TABLE 1. *COX activity and Caspase-3 activity of Cytc purified from pig brain tissue (ischemic/nonischemic)*

Type	Brain COX activity (min)	Caspase-3 activity (%)
Dephosphorylated brain Cyt*c* (ischemic)	283.5 ± 13.3 (100% ± 4.7)[a]	100 ± 4.3
Phosphorylated brain Cyt*c* (nonischemic)	147.5 ± 19.6* (52.0% ± 6.9)[a]	37.9 ± 16.1*

[a]Percentage of WT. *$P < 0.05$ compared with dephosphorylated Cyt*c*.

the unphosphorylated protein on a Phostag gel (Supplemental Fig. S1). Based on densitometry analysis, we report that about 35% of the protein was phosphorylated, which is likely an underestimation because of the delay in time extracting the organ that causes the tissue to become ischemic and to lose Cyt*c* phosphorylation (see Discussion).

S47E phosphomimetic Cytc as a model for S47 phosphorylation

To further functionally characterize the role of S47 phosphorylation, a recombinant phosphomimetic Cyt*c* mutant, S47E, was generated. Using a phosphomimetic mutant instead of *in vivo* phosphorylated Cyt*c* has the advantage that the modification cannot be lost during functional assays, especially those that require extended incubation times that could otherwise lead to hydrolysis of the phosphate group. In addition, essentially unlimited amounts can be generated by bacterial overexpression. The S47E mutant was purified along with recombinant WT and S47A Cyt*c*, a variant that cannot be phosphorylated, using a bacterial expression system (**Fig. 3*A***). The reduced and oxidized absorption spectra of these recombinant proteins were analyzed in order to confirm that the proteins were properly folded (Fig. 3*B*). The presence of the weak 695 nm peak of the oxidized spectra indicates the proper hexacoordinate structure of the heme iron (Fig. 3*B*, inset) (42). To effectively function as an electron carrier in the ETC, Cyt*c* must have a redox potential value between complex III and complex IV. The redox potential value for WT Cyt*c* was 272 ± 2 mV, which is similar to the values of 270 ± 1 mV and 256 ± 12 mV for S47A and S47E Cyt*c*, respectively (**Table 2**). These values lie within the literature values of mammalian Cyt*c* redox potential in the range of 220–270 mV (43, 44), suggesting that they can effectively participate in electron transfer.

Based on a published docking model of Cyt*c* and COX (45), S47 was suggested to interact with COX subunit VIIa (Fig. 3C). Brain and heart COX differ in their tissue-specific isoforms of subunits VIa, VIIa, and VIII (Fig. 2*B*). Therefore, COX activity with the Cyt*c* mutants was measured with both brain COX containing subunit VIIaL (liver-type) and heart COX containing subunit VIIaH (heart-type) to reveal potential kinetic differences of the 2 isozymes.

The COX activity in the presence of 5 μM phosphomimetic (S47E) Cyt*c* in reaction with pig brain COX was 54% lower compared with COX activity in the presence of 5 μM WT Cyt*c* (Table 2). These data suggest that S47E replacement is a good mimetic for *in vivo* S47 phosphorylation (Table 1). The S47A mutant resulted in COX activity values between the phosphomimetic and the WT, suggesting that this substitution does not optimally represent unphosphorylated WT Cyt*c*. The apparent K_m of Cyt*c* in the reaction with brain COX was 1.5, 1.4, and 1.5 μM for WT, S47A, and S47E Cyt*c*, respectively. With heart COX, phosphomimetic Cyt*c* resulted in partially inhibited respiration to an extent comparable with brain COX, suggesting that the tissue-specific isoforms of COX subunit VII in heart and brain do not modulate the effect of Cyt*c* S47 phosphorylation. The apparent K_m of Cyt*c* in the reaction with heart COX was 1.5, 1.2, and 1.5 μM for WT, S47A, and S47E Cyt*c*, respectively. However, COX activity of heart COX was 2.5 times lower than COX activity of brain COX (Table 2), which is consistent with other reports in the literature suggesting that liver-type COX has a higher turnover compared with heart-type COX, as reviewed in ref. (22).

In the presence of the phosphomimetic S47E replacement, caspase-3 activity was significantly inhibited (by 65%) compared with WT Cyt*c* (Table 2). The S47A mutant also resulted in significantly lower caspase-3 activity, suggesting that the hydroxyl group of the S47 residue is important for apoptotic activity and that any modification of this residue may affect the interaction of Cyt*c* with Apaf-1. In fact, the Apaf-1 Cyt*c* docking model (46) revealed that S47 is located in the Apaf-1 binding domain of Cyt*c* (Supplemental Fig. S2).

With increased ROS levels, Cyt*c* undergoes oxidative modifications such as sulfoxidation, which causes Cyt*c* to lose its function (47). This loss in function, upon addition of 3 mM H_2O_2, was monitored by a decrease in heme absorption of Cyt*c* at 408 nm. S47E Cyt*c* was about 30% more resistant to heme degradation by excess H_2O_2 compared with both WT and S47A Cyt*c*, suggesting that S47E Cyt*c* is more resistant to oxidative stress (Table 2).

As discussed in the Introduction, cardiolipin peroxidase activity is a proapoptotic function of Cyt*c*. Cardiolipin peroxidase activity was measured in the presence of cardiolipin, Cyt*c*, H_2O_2, and Amplex red as the fluorescence indicator of cardiolipin oxidation. In a 10:1 and 20:1 ratio of cardiolipin:Cyt*c*, WT Cyt*c* has the highest peroxidase activity compared with the S47A and S47E mutants (**Fig. 4**), further supporting the antiapoptotic function of the phosphorylated protein.

Crystal structure of S47E Cytc and molecular dynamics simulations

To gain a better understanding of the structure-function relationships of Cyt*c* when the S47 residue is modified, we

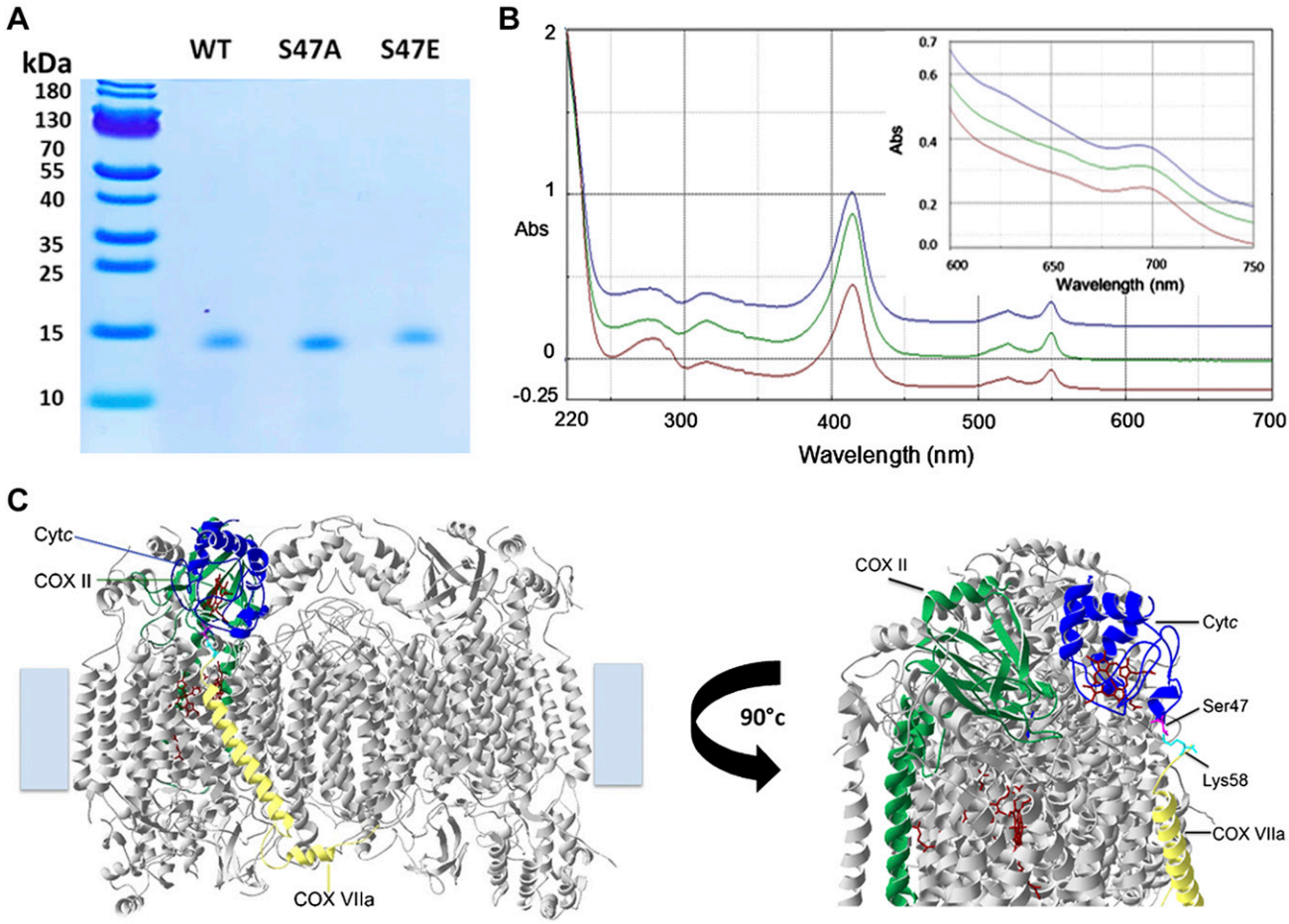

Figure 3. Characterization of recombinant WT, S47A, and S47E Cyt*c*. *A*) Coomassie gel of bacterially overexpressed and purified recombinant WT (lane 1), S47A (lane 2), and S47E (lane 3) Cyt*c* indicates that the proteins were purified to homogeneity. *B*) Reduced Cyt*c* (5 μM) spectra (220–700 nm) and oxidized Cyt*c* (100 μM) spectra (600–700 nm, inset) of recombinant WT (blue), S47A (red), and S47E (green) indicate correct folding and functionality of the proteins. *C*) Docking model of Cyt*c* and COX (45, 60). A COX residue within a distance of 3 Å from residue 47 (magenta) is highlighted (Lys58 of COX subunit VIIa, cyan). Abs, absorbance.

determined the crystal structure of S47E phosphomimetic Cyt*c* at 1.55 Å (Supplemental Table S1) and performed molecular dynamics simulations. The crystal structure of S47E (6N1O.pdb) frozen at 100 K is similar to the WT Cyt*c* structure (5C0Z.pdb) (**Fig. 5*A***). Phospho-S47 was superposed onto the Glu-47 residue of the S47E crystal structure (Fig. 5*B*) to demonstrate that S47E and phospho-S47 spatially arrange in a similar manner and that S47E is a good phosphomimetic model. Figure 5*C*–*F* shows the RMSD of the 4 molecules A, B, C, and D of the S47E Cyt*c* tetramer (6N1O.pdb) relative to the corresponding molecules A, B, C, and D of the WT Cytc tetramer (5C0Z.pdb). Increased RMSD was observed around the S47 residue; however, this was variable across the 4 molecules possibly because the S47E crystal structure was disordered with broken omit density especially in molecules C and D.

We performed molecular dynamics calculations to evaluate the possible effects of the mutations on the structrue of Cyt*c* in solution. WT Cyt*c* (5C0Z.pdb) and S47A, S47E, and phospho-S47 Cyt*c* modeled *in silico* from WT Cyt*c* (5C0Z.pdb) were run for 300 ns and divided into three 100-ns blocks. The first block was considered a pre-equilibrium period. The RMSD of the second block from 100 to 200 ns and third block from 200 to 300 ns were

TABLE 2. *Functional studies of WT, S47A, and S47E Cytc*

Cyt*c* variant	Brain COX activity (min)	Heart COX activity (min)	Caspase-3 activity (%)	Heme degradation (%)	Redox potential (mV)
WT	233.2 ± 15.1 (100% ± 6.5)[a]	98.1 ± 13.5 (100% ± 13.8)[a]	100 ± 1.9	100 ± 4.0	272 ± 2
S47A	192.3 ± 15.4* (82.5% ± 6.6)[a]	65.4 ± 14.6* (66.7% ± 14.9)[a]	38.0 ± 6.8*	99.5 ± 8.6	270 ± 1
S47E	106.6 ± 15.6* (45.7% ± 6.7)[a]	49.9 ± 2.7* (50.9% ± 2.8)[a]	35.5 ± 4.0*	67.5 ± 3.9*	256 ± 12

[a]Percentage of WT. *$P < 0.05$ compared with WT.

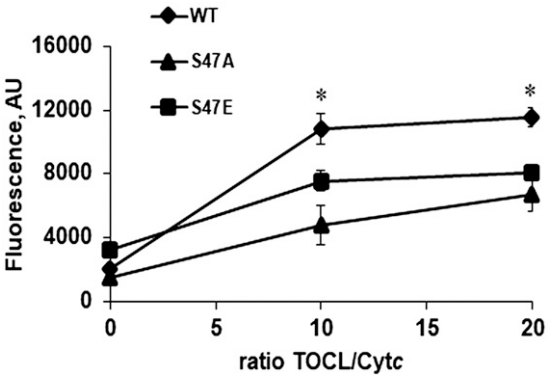

Figure 4. Cardiolipin peroxidase activity. Cardiolipin peroxidase activity is significantly lower with S47A and S47E Cyt*c* at 10:1 and 20:1 tetralinoleylcardiolipin (TOCL):Cyt*c* ratios compared with the WT.

plotted for the Cα position on each residue (Supplemental Fig. S3*A*–*D*). The molecular dynamics runs suggest that there is no major perturbation in the overall structure at Cyt*c* position 47 in S47A, S47E, and phospho-S47 molecules. However, the negative classic γ turn containing residues K27, T28, and G29 shows the highest RMSD, suggesting that this is the most unstable loop of Cyt*c*. Superposed WT Cyt*c* with S47A and S47E Cyt*c* shows that S47A (red) and S47E (cyan) Cyt*c* superpose well on top of each other, whereas the WT (blue) Cyt*c* structure is more deviated, especially around the loop containing T28 (Supplemental Fig. S3*E*).

DISCUSSION

Even though Cyt*c* is a well-studied protein and has been known for over a century, its regulation through cell signaling and post-translational modifications was only recently reported. This was made possible by improved protein purification protocols developed to preserve post-translational modifications and thus the physiologic regulatory properties of mitochondrial proteins including Cyt*c* and COX (13, 29). We previously identified tissue-specific phosphorylation sites of Cyt*c* in the heart (13), liver (14), and kidney (15). We also reported a phosphorylation site in the brain (Y97) that was induced by insulin treatment (16), but absent under basal conditions. Therefore, the basal phosphorylation state of Cyt*c* in the brain was unknown until this report. The brain is an organ that heavily depends on oxidative phosphorylation. In adult humans, the brain accounts for only about 2% of the body weight, yet it consumes 20% of the oxygen we breathe (48), making it the most energy expensive organ of the body.

Here, we show that Cyt*c* purified from pig brain is phosphorylated on residue S47. Cyt*c* is 95% conserved between human and pig, making the latter a good experimental model because of its close proteome resemblance to humans (49). In addition, we also mapped the same modification on immunoprecipitated Cyt*c* from rat brain tissue (data not shown), suggesting that it is the common regulatory post-translational modification present in the mammalian brain. To date, no studies have identified Cyt*c* S47 phosphorylation in the human brain, but S47 phosphorylation of Cyt*c* was mapped in 2 high-throughput phosphoproteomics studies from human skeletal muscle, suggesting that S47 phosphorylation is present in humans under normal physiologic conditions (17, 50). However, no functional follow-up studies were performed, and it is unclear if a meaningful fraction of the Cyt*c* protein pool contains this modification in skeletal muscle.

The Phos-tag gel data indicate that about 35% of the brain Cyt*c* pool was S47-phosphorylated, suggesting that this post-translational modification is biologically relevant. It should be noted that the observed fraction of phosphorylated Cyt*c* is likely an underestimation because of the time it takes to open the pig skull and snap freeze the brains, a period in which the tissue is ischemic and may lose some of this phosphorylation, which we know is completely lost after 1 h of ischemia. Thus, to overcome the challenge with regard to variability in phosphorylation of tissue-purified Cyt*c*, we used recombinant phosphomimetic (S47E) Cyt*c* for functional analyses. The phosphomimetic form behaved in a similar way to *in vivo* phosphorylated Cyt*c* in both COX activity and caspase-3 activity assays. In addition, the crystal structure of S47E Cyt*c*, obtained at a resolution of 1.55 Å, shows that it spatially arranges similarly to modeled phospho-S47 Cyt*c* (Fig. 5*B*), further supporting that S47E Cyt*c* serves as a good phosphomimetic model.

The S47 residue belongs to the Ω_{NY}-loop (foldon V) comprising residues 40–57, which were previously reported to have the highest unfolding capacity (51, 52). Furthermore, this is the loop that contains the only 2 disease-related mutations reported for Cyt*c* (G41S, Y48H) that cause thrombocytopenia in humans (53). This may further explain the substantial functional changes in respiration and apoptosis caused by single point mutations in this evolutionarily optimized protein. Surprisingly, RMSD analysis did not show a significant perturbation in the foldon V region of Cyt*c* containing S47 when phosphorylated or replaced with alanine or glutamate. However, significant changes in RMSD were observed around the T28 residue when S47 was modified. In contrast to most studies that report S47-containing Ω_{NY}-loop as the most unstable region of Cyt*c*, our molecular dynamics runs have suggested the T28-containing loop to be the most unstable portion of the protein. This loop is referred to as the "negative classic" γ turn of the protein comprising residues 27–29, which has been shown to be very important for the stability of Cyt*c* sidechains (54). Furthermore, we and others have previously reported that T28 is an important regulatory site of Cyt*c* that controls the ETC function (15, 55).

In several *in vitro* assays the control mutant, S47A Cyt*c*, behaved more like the phosphomimetic protein or showed a behavior somewhere between the two. This finding suggests that this specific site on Cyt*c* (*i.e.*, the presence of the Ser residue) is essential for maximal ETC electron flux and apoptotic activity. Even though alanine is the closest neutral replacement for a Ser residue, it lacks a polar group to mimic the hydroxyl group. We and others have observed effects deviating from the WT in some functional analysis with an alanine replacement in Cyt*c* (55). Recently

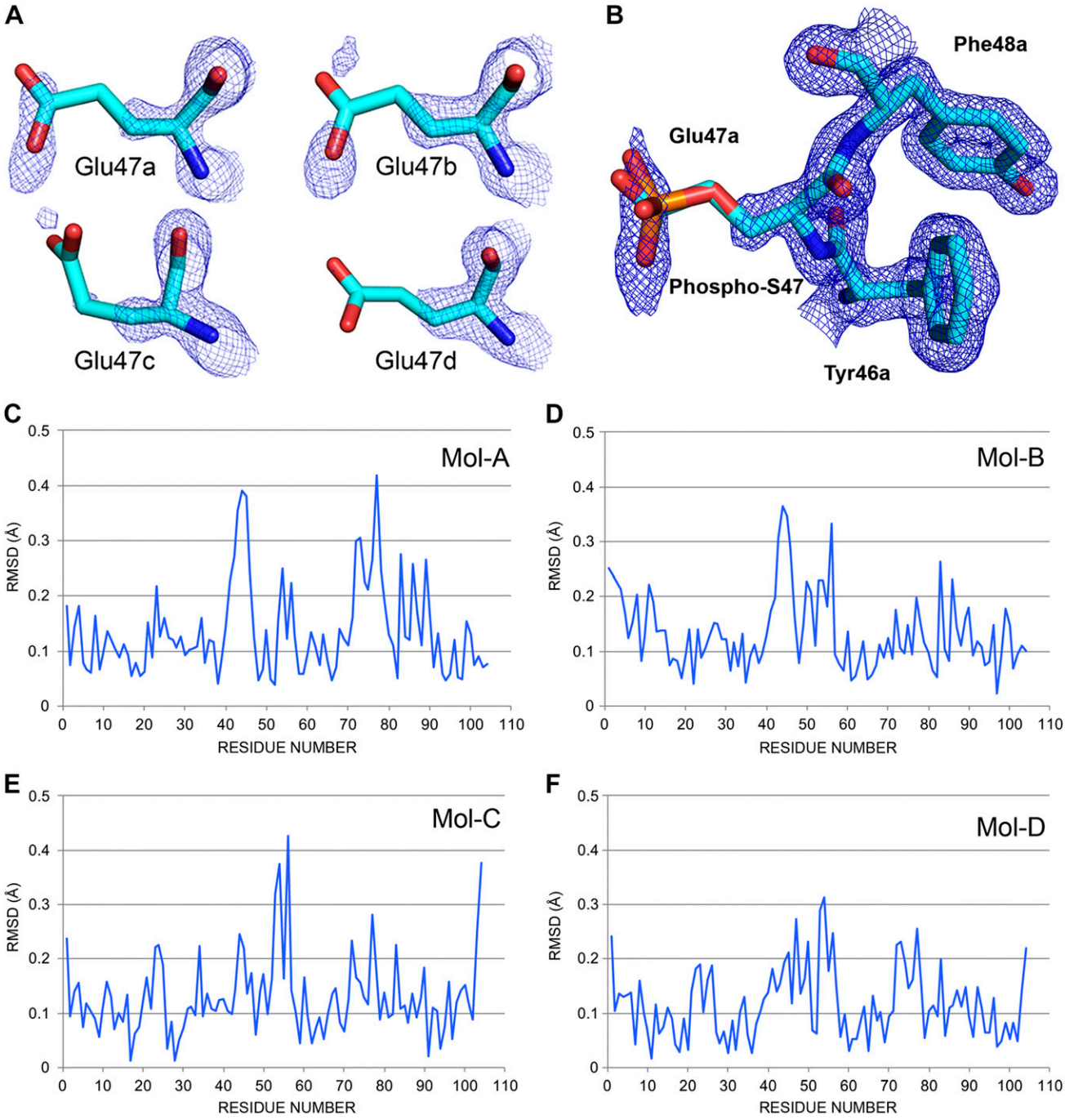

Figure 5. S47E crystal structure at 1.55 Å. *A*) Omit electron density for the S47E residues. The unbiased electron density calculated by Phenix.composite.omit and contoured at 1.0 RMSD with PyMOL is shown for the Glu-47 residues in the 4 Cyt*c* chains in the asymmetric unit of 6N1O.pdb. Cyt*c* S47E has 8 glutamate residues for a total of 32 in the 6N1O tetramer. They are on the surface, and most are mobile and disordered with broken omit density for the side chain atoms. If one counts the number of carboxyl group atoms (carbon δ, oxygen ε1. and oxygen ε2) in density at 1.0 RMSD in this figure then the numbers are E47a (3), E47b (1), E47c (0), and E47d (1). Applying this simple analysis to the entire crystal structure gives scores (maximum = 24) of 20, 17, 13, and 18, for chains A, B, C, and D, respectively. *B*) Phosphomimetic Glu-47. The $2F_o$-F_c electron density calculated by Coot (*https://www2.mrc-lmb.cam.ac.uk/personal/pemsley/coot/web/docs/coot.html*) from the 6N10 structure and data are shown for Phe-46a, Glu-47a, and Tyr-48a contoured at 1 RMSD (PyMOL). There are no residues within 3.5 Å of the Glu-47a side chain. The equivalent phospho-S47 sidechain is superposed onto Glu-47a to show the structural match. The phosphorus atom is orange. S47 was modeled by mutating Glu-47a back to a Ser with YASARA and then attaching a phosphate group with Coot. *C–F*) The RMSD figures comparing the 4 molecules A, B, C, and D of S47E (6N10.pdb) and WT (5C0Z.pdb) in the 2 crystal structures.

we reported similar behavior for another alanine mutant, T28A Cyt*c* (15). Superposition of WT, S47A, and S47E after 300 ns of molecular dynamics shows similar arrangement of S47A and S47E Cyt*c*. This may explain the similar functional effects observed for these 2 mutants in caspase-3 activity and cardiolipin peroxidation.

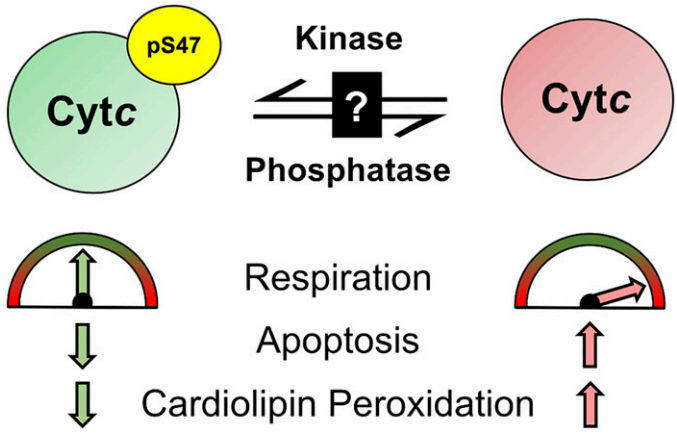

Figure 6. S47 phosphorylation (pS47) of Cyt*c* by an unknown kinase leads to intermediate healthy respiration, lower apoptosis, and lower cardiolipin peroxidase activity. Cyt*c* gets dephosphorylated under ischemia, which leads to pathologically high respiration rates, increased apoptosis, and increased cardiolipin peroxidase activity.

Interestingly, alanine substitution is found in position 47 across several different species such as *Drosophila*, fungi, algae, arthropods, and bacteria (56), indicating that an alanine replacement is evolutionarily permissible at this site. In fact, the presence of an alanine may be beneficial for these species since S47A demonstrates increased protective functions as observed with the phosphorylated protein, such as lower caspase-3 and cardiolipin peroxidase activities. The negatively charged amino acid aspartate, which is an alternative phosphomimetic replacement, was also found at this site in species such as snails, *Caenorhabditis elegans*, and nematodes (56). However, based on our crystallographic analysis, including the length of the phosphorylated side chain together with our functional data, we conclude that glutamate and not aspartate is the better phosphomimetic replacement to study Ser phosphorylation. This is also suggested by the fact that, despite S47D Cyt*c* showing lower caspase and cardiolipin peroxidase activities similar to S47E Cyt*c*, it behaves in an opposite manner in reaction with COX compared with *in vivo* phosphorylated or S47E Cyt*c*, leading to about a 70% increase in respiration (55). In contrast, the glutamate phosphomimetic reflects the activity seen with the *in vivo* phosphorylated protein.

COX along with Cyt*c* are evolutionarily adapted to meet tissue-specific energy needs of different organs. One adaptive mechanism is the expression of tissue-specific isoforms, such as the liver-type and heart and skeletal muscle-type specific isoforms in COX subunits VIa, VIIa, and VIII (22). Heart-type COX is specific to the heart and skeletal muscle tissue, whereas the liver-type is expressed in most other tissues (57, 58). The liver-type isoforms are expressed in tissues such as the liver and brain that have specialized functions and not such a high capacity for mitochondria compared with heart and skeletal muscle. Therefore, liver-type COX has a higher basal activity compared with heart-type COX (22). However, the *in vitro* COX activity experimental setup used for these measurements do not take into account the $\Delta\Psi_m$ and supercomplex formation of the ETC complexes, which are important features of intact mitochondria. Therefore, in order to better represent the physiologic *in vivo* situation, COX activity should be measured in live cells or tissues. Because COX subunit VIIa was suggested to interact with S47 of Cyt*c* based on a computational docking model (45), we asked whether the effect of the Cyt*c* S47 modification on COX activity may be further modulated by the presence of the liver- *vs.* the heart-type isoform of subunit VIIa. Surprisingly, both heart and brain COX showed a similar level of inhibition of respiration with phosphomimetic Cyt*c* compared with WT, suggesting that interaction of Cyt*c* with subunit VIIa does not alter the respiration rate in a tissue-specific manner.

In summary, this is the first study reporting the basal phosphorylation state of Cyt*c* in the mammalian brain and its functional characterization using both *in vivo* phosphorylated and phosphomimetic (S47E) Cyt*c*. Our results suggest that this modification is cytoprotective in terms of maintaining optimal intermediate mitochondrial respiration rates by partially inhibiting COX activity (**Fig. 6**). We propose that the loss of this post-translational modification during cellular stress, such as during brain ischemia (Fig. 2*A*), would cause pathologically high respiration rates during reperfusion that would lead to $\Delta\Psi_m$ hyperpolarization and a ROS burst, promoting cardiolipin peroxidation and triggering apoptosis (24). Lower caspase-3 and cardiolipin peroxidase activities provide another safeguard mechanism from apoptosis when Cyt*c* is phosphorylated. These mechanisms should be further investigated in an *in vivo* model. In addition, the kinase and phosphatase involved in this signaling pathway are yet to be discovered. A small number of kinases and phosphatases with localization to brain mitochondria has been reported (59), further supporting tissue-specific phosphorylation of mitochondrial proteins. We propose that a better understanding of Cyt*c* regulation in the brain may facilitate the development of a Cyt*c*-targeted neuroprotective therapy to improve debilitating pathologies such as ischemic stroke when Cyt*c* becomes dephosphorylated. FJ

ACKNOWLEDGMENTS

This work was supported by the U.S. National Institutes of Health (NIH) National Institute of General Medical Sciences Grants R01 GM116807 and R01 GM113908, NIH National Institute of Neurological Disorders and Stroke Grants R01 NS091242 and R42 NS105238, and by the Office of the Assistant Secretary of Defense for Health Affairs through the

Peer Reviewed Medical Research Program under Award W81XWH-16-1-0175. Opinions, interpretations, conclusions, and recommendations are those of the authors and are not necessarily endorsed by the funding agencies including the Department of Defense or the NIH. This research used resources of the Advanced Photon Source, a U.S. Department of Energy Office of Science User Facility operated for the Department of Energy Office of Science by Argonne National Laboratory under Contract DE-AC02- 06CH11357. Use of the Life Sciences Collaborative Access Team (LS-CAT) Sector 21 was supported by the Michigan Economic Development Corp., the Michigan Technology Tri-Corridor (Grant 085P1000817), and Wayne State University Office of the Vice-President for Research. The authors declare no conflicts of interest.

AUTHOR CONTRIBUTIONS

H. A. Kalpage, J. Liu, A. Varughese, J. Wan, A. A. Turner, Q. Ji, M. P. Zurek, A. A. Kapralov, I. Lee, and M. Hüttemann designed and performed experiments; H. A. Kalpage and M. Hüttemann wrote the manuscript; A. Vaishnav, J. S. Brunzelle, and B. F. P. Edwards determined the crystal structures; V. E. Kagan, L. I. Grossman, T. H. Sanderson, A. R. Salomon, B. F. P. Edwards, and M. Hüttemann assisted with the experimental design and supervised the project; and all authors edited and approved the final version of the manuscript.

REFERENCES

1. Piccoli, C., Scrima, R., Boffoli, D., and Capitanio, N. (2006) Control by cytochrome c oxidase of the cellular oxidative phosphorylation system depends on the mitochondrial energy state. *Biochem. J.* **396**, 573–583
2. Dalmonte, M. E., Forte, E., Genova, M. L., Giuffrè, A., Sarti, P., and Lenaz, G. (2009) Control of respiration by cytochrome c oxidase in intact cells: role of the membrane potential. *J. Biol. Chem.* **284**, 32331–32335
3. Hinkle, P. C., Kumar, M. A., Resetar, A., and Harris, D. L. (1991) Mechanistic stoichiometry of mitochondrial oxidative phosphorylation. *Biochemistry* **30**, 3576–3582
4. Hüttemann, M., Pecina, P., Rainbolt, M., Sanderson, T. H., Kagan, V. E., Samavati, L., Doan, J. W., and Lee, I. (2011) The multiple functions of cytochrome c and their regulation in life and death decisions of the mammalian cell: from respiration to apoptosis. *Mitochondrion* **11**, 369–381
5. Kagan, V. E., Tyurin, V. A., Jiang, J., Tyurina, Y. Y., Ritov, V. B., Amoscato, A. A., Osipov, A. N., Belikova, N. A., Kapralov, A. A., Kini, V., Vlasova, I. I., Zhao, Q., Zou, M., Di, P., Svistunenko, D. A., Kurnikov, I. V., and Borisenko, G. G. (2005) Cytochrome c acts as a cardiolipin oxygenase required for release of proapoptotic factors. *Nat. Chem. Biol.* **1**, 223–232
6. Kagan, V. E., Bayir, H. A., Belikova, N. A., Kapralov, O., Tyurina, Y. Y., Tyurin, V. A., Jiang, J., Stoyanovsky, D. A., Wipf, P., Kochanek, P. M., Greenberger, J. S., Pitt, B., Shvedova, A. A., and Borisenko, G. (2009) Cytochrome c/cardiolipin relations in mitochondria: a kiss of death. *Free Radic. Biol. Med.* **46**, 1439–1453
7. Schlame, M., Rua, D., and Greenberg, M. L. (2000) The biosynthesis and functional role of cardiolipin. *Prog. Lipid Res.* **39**, 257–288
8. Kagan, V. E., Borisenko, G. G., Tyurina, Y. Y., Tyurin, V. A., Jiang, J., Potapovich, A. I., Kini, V., Amoscato, A. A., and Fujii, Y. (2004) Oxidative lipidomics of apoptosis: redox catalytic interactions of cytochrome c with cardiolipin and phosphatidylserine. *Free Radic. Biol. Med.* **37**, 1963–1985
9. Kagan, V. E., Tyurina, Y. Y., Bayir, H., Chu, C. T., Kapralov, A. A., Vlasova, I. I., Belikova, N. A., Tyurin, V. A., Amoscato, A., Epperly, M., Greenberger, J., Dekosky, S., Shvedova, A. A., and Jiang, J. (2006) The "pro-apoptotic genies" get out of mitochondria: oxidative lipidomics and redox activity of cytochrome c/cardiolipin complexes. *Chem. Biol. Interact.* **163**, 15–28
10. Giorgio, M., Migliaccio, E., Orsini, F., Paolucci, D., Moroni, M., Contursi, C., Pelliccia, G., Luzi, L., Minucci, S., Marcaccio, M., Pinton, P., Rizzuto, R., Bernardi, P., Paolucci, F., and Pelicci, P. G. (2005) Electron transfer between cytochrome c and p66Shc generates reactive oxygen species that trigger mitochondrial apoptosis. *Cell* **122**, 221–233
11. Pereverzev, M. O., Vygodina, T. V., Konstantinov, A. A., and Skulachev, V. P. (2003) Cytochrome c, an ideal antioxidant. *Biochem. Soc. Trans.* **31**, 1312–1315
12. Kalpage, H. A., Bazylianska, V., Recanati, M. A., Fite, A., Liu, J., Wan, J., Mantena, N., Malek, M. H., Podgorski, I., Heath, E. I., Vaishnav, A., Edwards, B. F., Grossman, L. I., Sanderson, T. H., Lee, I., and Hüttemann, M. (2019) Tissue-specific regulation of cytochrome c by post-translational modifications: respiration, the mitochondrial membrane potential, ROS, and apoptosis. *FASEB J.* **33**, 1540–1553
13. Lee, I., Salomon, A. R., Yu, K., Doan, J. W., Grossman, L. I., and Hüttemann, M. (2006) New prospects for an old enzyme: mammalian cytochrome *c* is tyrosine-phosphorylated in vivo. *Biochemistry* **45**, 9121–9128
14. Yu, H., Lee, I., Salomon, A. R., Yu, K., and Hüttemann, M. (2008) Mammalian liver cytochrome *c* is tyrosine-48 phosphorylated in vivo, inhibiting mitochondrial respiration. *Biochim. Biophys. Acta* **1777**, 1066–1071
15. Mahapatra, G., Varughese, A., Ji, Q., Lee, I., Liu, J., Vaishnav, A., Sinkler, C., Kapralov, A. A., Moraes, C. T., Sanderson, T. H., Stemmler, T. L., Grossman, L. I., Kagan, V. E., Brunzelle, J. S., Salomon, A. R., Edwards, B. F., and Hüttemann, M. (2017) Phosphorylation of cytochrome c threonine 28 regulates electron transport chain activity in kidney: implications for AMP kinase. *J. Biol. Chem.* **292**, 64–79
16. Sanderson, T. H., Mahapatra, G., Pecina, P., Ji, Q., Yu, K., Sinkler, C., Varughese, A., Kumar, R., Bukowski, M. J., Tousignant, R. N., Salomon, A. R., Lee, I., and Hüttemann, M. (2013) Cytochrome C is tyrosine 97 phosphorylated by neuroprotective insulin treatment. *PLoS One* **8**, e78627
17. Zhao, X., León, I. R., Bak, S., Mogensen, M., Wrzesinski, K., Højlund, K., and Jensen, O. N. (2011) Phosphoproteome analysis of functional mitochondria isolated from resting human muscle reveals extensive phosphorylation of inner membrane protein complexes and enzymes. *Mol. Cell Proteomics* **10**, M110.000299
18. Hoffman, N. J., Parker, B. L., Chaudhuri, R., Fisher-Wellman, K. H., Kleinert, M., Humphrey, S. J., Yang, P., Holliday, M., Trefely, S., Fazakerley, D. J., Stöckli, J., Burchfield, J. G., Jensen, T. E., Jothi, R., Kiens, B., Wojtaszewski, J. F., Richter, E. A., and James, D. E. (2015) Global phosphoproteomic analysis of human skeletal muscle reveals a network of exercise-regulated kinases and AMPK substrates. *Cell Metab.* **22**, 922–935; erratum: 948
19. Pierron, D., Opazo, J. C., Heiske, M., Papper, Z., Uddin, M., Chand, G., Wildman, D. E., Romero, R., Goodman, M., and Grossman, L. I. (2011) Silencing, positive selection and parallel evolution: busy history of primate cytochromes C. *PLoS One* **6**, e26269
20. Hüttemann, M., Jaradat, S., and Grossman, L. I. (2003) Cytochrome *c* oxidase of mammals contains a testes-specific isoform of subunit VIb–the counterpart to testes-specific cytochrome *c*? *Mol. Reprod. Dev.* **66**, 8–16
21. Pierron, D., Wildman, D. E., Hüttemann, M., Letellier, T., and Grossman, L. I. (2012) Evolution of the couple cytochrome c and cytochrome c oxidase in primates. *Adv. Exp. Med. Biol.* **748**, 185–213
22. Sinkler, C. A., Kalpage, H., Shay, J., Lee, I., Malek, M. H., Grossman, L. I., and Hüttemann, M. (2017) Tissue- and condition-specific isoforms of mammalian cytochrome *c* oxidase subunits: from function to human disease. *Oxid. Med. Cell. Longev.* **2017**, 1534056
23. Helling, S., Hüttemann, M., Ramzan, R., Kim, S. H., Lee, I., Müller, T., Langenfeld, E., Meyer, H. E., Kadenbach, B., Vogt, S., and Marcus, K. (2012) Multiple phosphorylations of cytochrome c oxidase and their functions. *Proteomics* **12**, 950–959
24. Sanderson, T. H., Reynolds, C. A., Kumar, R., Przyklenk, K., and Hüttemann, M. (2013) Molecular mechanisms of ischemia-reperfusion injury in brain: pivotal role of the mitochondrial membrane potential in reactive oxygen species generation. *Mol. Neurobiol.* **47**, 9–23
25. Liu, S. S. (1999) Cooperation of a "reactive oxygen cycle" with the Q cycle and the proton cycle in the respiratory chain–superoxide generating and cycling mechanisms in mitochondria. *J. Bioenerg. Biomembr.* **31**, 367–376
26. Korshunov, S. S., Skulachev, V. P., and Starkov, A. A. (1997) High protonic potential actuates a mechanism of production of reactive oxygen species in mitochondria. *FEBS Lett.* **416**, 15–18

27. Hüttemann, M., Lee, I., Pecinova, A., Pecina, P., Przyklenk, K., and Doan, J. W. (2008) Regulation of oxidative phosphorylation, the mitochondrial membrane potential, and their role in human disease. *J. Bioenerg. Biomembr.* **40**, 445–456
28. Rottenberg, H., Covian, R., and Trumpower, B. L. (2009) Membrane potential greatly enhances superoxide generation by the cytochrome bc1 complex reconstituted into phospholipid vesicles. *J. Biol. Chem.* **284**, 19203–19210
29. Lee, I., Salomon, A. R., Yu, K., Samavati, L., Pecina, P., Pecinova, A., and Hüttemann, M. (2009) Isolation of regulatory-competent, phosphorylated cytochrome *C* oxidase. *Methods Enzymol.* **457**, 193–210
30. Pecina, P., Borisenko, G. G., Belikova, N. A., Tyurina, Y. Y., Pecinova, A., Lee, I., Samhan-Arias, A. K., Przyklenk, K., Kagan, V. E., and Hüttemann, M. (2010) Phosphomimetic substitution of cytochrome C tyrosine 48 decreases respiration and binding to cardiolipin and abolishes ability to trigger downstream caspase activation. *Biochemistry* **49**, 6705–6714
31. Margoliash, E., and Frohwirt, N. (1959) Spectrum of horse-heart cytochrome c. *Biochem. J.* **71**, 570–572
32. Liu, Z., Lin, H., Ye, S., Liu, Q. Y., Meng, Z., Zhang, C. M., Xia, Y., Margoliash, E., Rao, Z., and Liu, X. J. (2006) Remarkably high activities of testicular cytochrome c in destroying reactive oxygen species and in triggering apoptosis. *Proc. Natl. Acad. Sci. USA* **103**, 8965–8970
33. Kadenbach, B., Jarausch, J., Hartmann, R., and Merle, P. (1983) Separation of mammalian cytochrome c oxidase into 13 polypeptides by a sodium dodecyl sulfate-gel electrophoretic procedure. *Anal. Biochem.* **129**, 517–521
34. Kabsch, W. (2010) Xds. *Acta Crystallogr. D Biol. Crystallogr.* **66**, 125–132
35. Vonrhein, C., Flensburg, C., Keller, P., Sharff, A., Smart, O., Paciorek, W., Womack, T., and Bricogne, G. (2011) Data processing and analysis with the autoPROC toolbox. *Acta Crystallogr. D Biol. Crystallogr.* **67**, 293–302
36. Adams, P. D., Afonine, P. V., Bunkóczi, G., Chen, V. B., Davis, I. W., Echols, N., Headd, J. J., Hung, L. W., Kapral, G. J., Grosse-Kunstleve, R. W., McCoy, A. J., Moriarty, N. W., Oeffner, R., Read, R. J., Richardson, D. C., Richardson, J. S., Terwilliger, T. C., and Zwart, P. H. (2010) PHENIX: a comprehensive Python-based system for macromolecular structure solution. *Acta Crystallogr. D Biol. Crystallogr.* **66**, 213–221
37. Joosten, R. P., Long, F., Murshudov, G. N., and Perrakis, A. (2014) The PDB_REDO server for macromolecular structure model optimization. *IUCrJ* **1**, 213–220
38. Krieger, E., and Vriend, G. (2015) New ways to boost molecular dynamics simulations. *J. Comput. Chem.* **36**, 996–1007
39. Hornak, V., Abel, R., Okur, A., Strockbine, B., Roitberg, A., and Simmerling, C. (2006) Comparison of multiple Amber force fields and development of improved protein backbone parameters. *Proteins* **65**, 712–725
40. Michel, B., and Bosshard, H. R. (1984) Spectroscopic analysis of the interaction between cytochrome c and cytochrome c oxidase. *J. Biol. Chem.* **259**, 10085–10091
41. Kuhn-Nentwig, L., and Kadenbach, B. (1985) Isolation and properties of cytochrome c oxidase from rat liver and quantification of immunological differences between isozymes from various rat tissues with subunit-specific antisera. *Eur. J. Biochem.* **149**, 147–158
42. Dickerson, R., and Timkovich, R. (1975) Cytochrome c. In *The Enzymes* (Boyer, P. D., ed.), **Vol. 11**, pp. 397–472, Academic Press, New York
43. Cammack, R. (1995) Redox states and potentials. In *Bioenergetics - A Practical Approach* (Brown, G. C., and Cooper, C. E., eds.), pp. 93–95, IRL Press, Oxford, United Kingdom
44. Nicholls, D. G., and Ferguson, S. J. (1992) *Bioenergetics 2*, Academic Press Limited, London, San Diego
45. Roberts, V. A., and Pique, M. E. (1999) Definition of the interaction domain for cytochrome c on cytochrome c oxidase. III. Prediction of the docked complex by a complete, systematic search. *J. Biol. Chem.* **274**, 38051–38060
46. Cheng, T. C., Hong, C., Akey, I. V., Yuan, S., and Akey, C. W. (2016) A near atomic structure of the active human apoptosome. *eLife* **5**, e17755
47. Hannibal, L., Tomasina, F., Capdevila, D. A., Demicheli, V., Tórtora, V., Alvarez-Paggi, D., Jemmerson, R., Murgida, D. H., and Radi, R. (2016) Alternative conformations of cytochrome c: structure, function, and detection. *Biochemistry* **55**, 407–428
48. Raichle, M. E., and Gusnard, D. A. (2002) Appraising the brain's energy budget. *Proc. Natl. Acad. Sci. USA* **99**, 10237–10239
49. Bassols, A., Costa, C., Eckersall, P. D., Osada, J., Sabrià, J., and Tibau, J. (2014) The pig as an animal model for human pathologies: a proteomics perspective. *Proteomics Clin. Appl.* **8**, 715–731
50. Højlund, K., Bowen, B. P., Hwang, H., Flynn, C. R., Madireddy, L., Geetha, T., Langlais, P., Meyer, C., Mandarino, L. J., and Yi, Z. (2009) In vivo phosphoproteome of human skeletal muscle revealed by phosphopeptide enrichment and HPLC-ESI-MS/MS. *J. Proteome Res.* **8**, 4954–4965
51. Maity, H., Maity, M., and Englander, S. W. (2004) How cytochrome c folds, and why: submolecular foldon units and their stepwise sequential stabilization. *J. Mol. Biol.* **343**, 223–233
52. Karsisiotis, A. I., Deacon, O. M., Wilson, M. T., Macdonald, C., Blumenschein, T. M., Moore, G. R., and Worrall, J. A. (2016) Increased dynamics in the 40-57 Ω-loop of the G41S variant of human cytochrome c promote its pro-apoptotic conformation. *Sci. Rep.* **6**, 30447
53. Deacon, O. M., Svistunenko, D. A., Moore, G. R., Wilson, M. T., and Worrall, J. A. R. (2018) Naturally occurring disease-related mutations in the 40-57 Ω-Loop of human cytochrome c control triggering of the alkaline isomerization. *Biochemistry* **57**, 4276–4288
54. Sanishvili, R., Volz, K. W., Westbrook, E. M., and Margoliash, E. (1995) The low ionic strength crystal structure of horse cytochrome c at 2.1 A resolution and comparison with its high ionic strength counterpart. *Structure* **3**, 707–716
55. Guerra-Castellano, A., Díaz-Moreno, I., Velázquez-Campoy, A., De la Rosa, M. A., and Díaz-Quintana, A. (2016) Structural and functional characterization of phosphomimetic mutants of cytochrome c at threonine 28 and serine 47. *Biochim. Biophys. Acta* **1857**, 387–395
56. Zaidi, S., Hassan, M. I., Islam, A., and Ahmad, F. (2014) The role of key residues in structure, function, and stability of cytochrome-c. *Cell. Mol. Life Sci.* **71**, 229–255
57. Hüttemann, M., Mühlenbein, N., Schmidt, T. R., Grossman, L. I., and Kadenbach, B. (2000) Isolation and sequence of the human cytochrome c oxidase subunit VIIaL gene. *Biochim. Biophys. Acta* **1492**, 252–258
58. Jaradat, S. A., Ko, M. S., and Grossman, L. I. (1998) Tissue-specific expression and mapping of the Cox7ah gene in mouse. *Genomics* **49**, 363–370
59. Arachiche, A., Augereau, O., Decossas, M., Pertuiset, C., Gontier, E., Letellier, T., and Dachary-Prigent, J. (2008) Localization of PTP-1B, SHP-2, and Src exclusively in rat brain mitochondria and functional consequences. *J. Biol. Chem.* **283**, 24406–24411
60. Tsukihara, T., Aoyama, H., Yamashita, E., Tomizaki, T., Yamaguchi, H., Shinzawa-Itoh, K., Nakashima, R., Yaono, R., and Yoshikawa, S. (1996) The whole structure of the 13-subunit oxidized cytochrome c oxidase at 2.8 A. *Science* **272**, 1136–1144

Received for publication May 2, 2019.
Accepted for publication August 26, 2019.